Climatic Change (2023) 176:105
https://doi.org/10.1007/s10584-023-03585-2

Extreme events in the multi-proxy South Pacific drought atlas

Philippa A. Higgins[1,2,3] · **Jonathan G. Palmer**[2,4] · **Martin S. Andersen**[5] · **Christian S. M. Turney**[2,3,4] · **Fiona Johnson**[1,6]

Received: 12 December 2022 / Accepted: 13 July 2023 / Published online: 24 July 2023

Abstract

Droughts are a natural occurrence in many small Pacific Islands and can have severe impacts on local populations and environments. The El Niño-Southern Oscillation (ENSO) is a well-known driver of drought in the South Pacific, but our understanding of extreme ENSO events and their influence on island hydroclimate is limited by the short instrumental record and the infrequency of ENSO extremes. To address this gap, we developed the South Pacific Drought Atlas (SPaDA), a multi-proxy, spatially resolved reconstruction of the November–April Standardised Precipitation Evapotranspiration Index for the southwest Pacific islands. The reconstruction covers the period from 1640 to 1998 CE and is based on nested principal components regression. It replicates historical droughts linked to ENSO events with global influence, compares well to previously published ENSO reconstructions, and is independently verified against fossil coral records from the Pacific. To identify anomalous hydroclimatic states in the SPaDA that may indicate the occurrence of an extreme event, we used an Isolation Forest, an unsupervised machine learning algorithm. Extreme El Niño events characterised by very strong southwest Pacific drought anomalies and a zonal SPCZ orientation are shown to have occurred throughout the reconstruction interval, providing a valuable baseline to compare to climate model projections. By identifying the spatial patterns of drought resulting from extreme events, we can better understand the impacts these events may have on individual Pacific Islands in the future.

Keywords Paleoclimate · Reconstruction · Anomaly detection · Water resources

✉ Philippa A. Higgins
philippa.higgins@unsw.edu.au

[1] Water Research Centre, School of Civil and Environmental Engineering, University of New South Wales, Kensington, Australia

[2] ARC Centre of Excellence in Australian Biodiversity and Heritage, University of New South Wales, Kensington, Australia

[3] Division of Research, University of Technology Sydney, Sydney, Australia

[4] Chronos 14Carbon-Cycle Facility, Mark Wainwright Analytical Centre, University of New South Wales, Kensington, Australia

[5] Water Research Laboratory, School of Civil and Environmental Engineering, University of New South Wales, Kensington, Australia

[6] ARC Training Centre in Data Science for Resources and Environments, Sydney, Australia

1 Introduction

South Pacific Island countries are highly vulnerable to extreme events such as droughts, which impact water availability, food security, public health, and economic activity (Annamalai et al. 2015; Iese et al. 2021). While extreme events are a natural occurrence over much of the South Pacific, due to the influence of the El Niño-Southern Oscillation (ENSO), the small size and remote location of many Pacific islands provide limited opportunities to buffer the impacts of climate extremes (Johnson et al. 2021).

The spatial distribution of precipitation—and drought—over the South Pacific is mostly controlled by the position and movement of two large bands of low atmospheric pressure, the Intertropical Convergence Zone (ITCZ) and the South Pacific Convergence Zone (SPCZ). Shifts in the mean position of these convergence zones, modulated by interannual fluctuations in ENSO and longer-term variability from the Interdecadal Pacific Oscillation (IPO), strongly influence moisture availability across the region (Ludert et al. 2018; McGree et al. 2016; Power et al. 1999). An equatorward movement of the convergence zones during El Niño events and positive phases of the IPO increases the likelihood of drought in the southwestern Pacific. Conversely, during La Niña events and negative IPO phases, the SPCZ and ITCZ move away from the equator, making drought conditions more likely for the more peripheral islands lying at the northeast end of the South Pacific region (McGree et al. 2016; van der Wiel et al. 2016). The extreme shifts in the position and intensity of the ITCZ and SPCZ during strong ENSO events can have devastating impacts across the region and globally (Rifai et al. 2019).

Despite a substantial body of research into the climate drivers affecting South Pacific drought (Capotondi et al. 2015; McPhaden et al. 2006), the quantification and attribution of historical drought trends and variability remains a research gap due to limited data availability (Iese et al. 2021). Climate records for the Pacific region are generally sparse, with robust meteorological records only available from the 1950s for many islands (Lorrey et al. 2012). The instrumental record is thus too short to assess past trends and variability in droughts across the region. Our understanding of extreme ENSO events and their impact on Pacific Island drought is further limited by their infrequency, with only five events occurring during the satellite era (Santoso et al. 2017). Climate models suggest both the frequency and intensity of ENSO events have increased in the industrial age (Power et al. 2017), and extreme ENSO events are projected to increase in frequency with global warming (Cai et al. 2012, 2014). Projected climate change impacts mean that droughts will be an issue of increased concern for the Pacific Islands in the future (Iese et al. 2021).

Documentary records have greatly enhanced our understanding of drought occurrence prior to the instrumental period and are the best source for information on the effects of drought on societies (Brázdil et al. 2018). Substantial research effort has been expended to identify and digitise documentary climate information for the Pacific Islands. D'Aubert and Nunn (2012) collated the most extensive record of historical drought in the Pacific to date, covering the period 1722–1987. However, it is not a complete record, because drought information is challenging to identify in historical documents and records are unevenly distributed over the different island groups and through time (D'Aubert & Nunn, 2012).

Another data source capable of providing spatially resolved drought records at high temporal resolution are paleoclimate proxies (Brázdil et al. 2018). There is a long history of utilising moisture-sensitive tree rings to develop records of growing season drought in many parts of the world. The compilations of such records to cover spatial areas are commonly referred to as 'drought atlases' (Cook et al. 1999, 2010a; Morales et al. 2020; Stahle

et al. 2016). Multi-proxy drought atlases, which integrate tree rings with other proxy datasets such as corals (Palmer et al. 2015) or documentary records (Cook et al. 2015), leverage the benefits of multiple proxies to provide a more complete picture of past hydro-climatological change.

In this study, we present the first spatially resolved, multi-proxy drought atlas reconstruction for the South Pacific islands. This new reconstruction, the South Pacific Drought Atlas (SPaDA), utilises tropical coral records from the centre of ENSO action along with tree ring records to reconstruct drought over the last 350 years. The reconstruction is verified against existing paleoclimate reconstructions from the region and then used to document the spatial extent and severity of extreme droughts previously identified in documentary records. The SPaDA provides an extended, continuous dataset of climate information, which can be used to explore the occurrence of extreme events in the pre-instrumental period. To demonstrate the value of the SPaDA, we show how anomalous drought patterns can be used to help identify past ENSO extremes both in time and in space, providing a multi-centennial context for their occurrence.

2 Data and methods

2.1 Climate data

The reconstruction target was the Standardised Precipitation Evapotranspiration Index (SPEI; (Vicente-Serrano et al. 2010)), a water-balance-based drought index previously used in paleo-drought reconstructions (Seftigen et al. 2015; Tejedor et al. 2017). The SPEI was selected as the drought index because it is easy to compute, has minimal input data requirements, and is a multi-scalar index, which prevents bias towards the wet season in regions with strong wet/dry seasonality like the Pacific (Romero et al. 2020). To calculate SPEI, monthly values of precipitation minus potential evapotranspiration are calculated and summed over the timescale of interest. SPEI is then obtained by fitting a log-logistic probability distribution function to the series and transforming it to a standardised normal distribution with reference to a baseline period (Beguería et al. 2014; Vicente-Serrano et al. 2010). The potential evapotranspiration component of the SPEI was calculated according to the method of Thornthwaite (1948), which only requires monthly precipitation and temperature. More complex methods for estimating evapotranspiration are unsuitable for a South Pacific–wide study as most stations lack data for additional meteorological parameters. The Thornthwaite method therefore provides a consistent approach for the entire region.

Monthly precipitation and temperature data for Pacific Island meteorological stations were sourced from the Climatic Research Unit (University of East Anglia) and Met Office CRU TS version 4.04 database (Harris et al. 2020). Data for islands not included in the CRU TS v4.04 database (Willis Is., Norfolk Is., Raoul Is., Pitcairn Is., and Nauru) was sourced from the relevant meteorological agencies. A long baseline period (i.e. more than 30 and ideally more than 50 years) that captures natural variability is required to calculate SPEI (Vicente-Serrano et al. 2010). Data availability for Pacific Islands varies through time, with the number of stations increasing rapidly following World War Two but decreasing after 1990 (Figure S1). The baseline period, 1960–1990, was selected to maximise both the number of stations with data and their geographical coverage. Gauges with less than

30 years of data (e.g. Honiara, Solomon Islands) were excluded from the study (Figure S1). Thus, the SPaDA does not extend to cover all South Pacific Island nations.

Rather than computing SPEI directly from gauge data, the grid points associated with the gauge stations were extracted from the CRU TS v4.04 gridded precipitation and temperature datasets. Using the gridded data takes advantage of the CRU methodology (see Harris et al. 2020) to fill short data gaps (one to several months). We did not extend the reconstruction domain to islands with CRU grid points but without meteorological station data over the baseline period due to data quality issues.

2.2 Proxy network

Most of the high-resolution proxy records located in the southwest Pacific are from corals. Six Pacific Ocean coral records and one coral luminesce chronology from the Great Barrier Reef (Fig. 1, Table S1) which have the first year of record before 1800 CE and are continuous until or after 1998 CE were selected from the PAGES OCEAN2K database (Lough et al. 2015; Tierney et al. 2015). One annually dated speleothem record from Vanuatu was also included in the predictor pool (Partin et al. 2013). Monthly resolution coral records

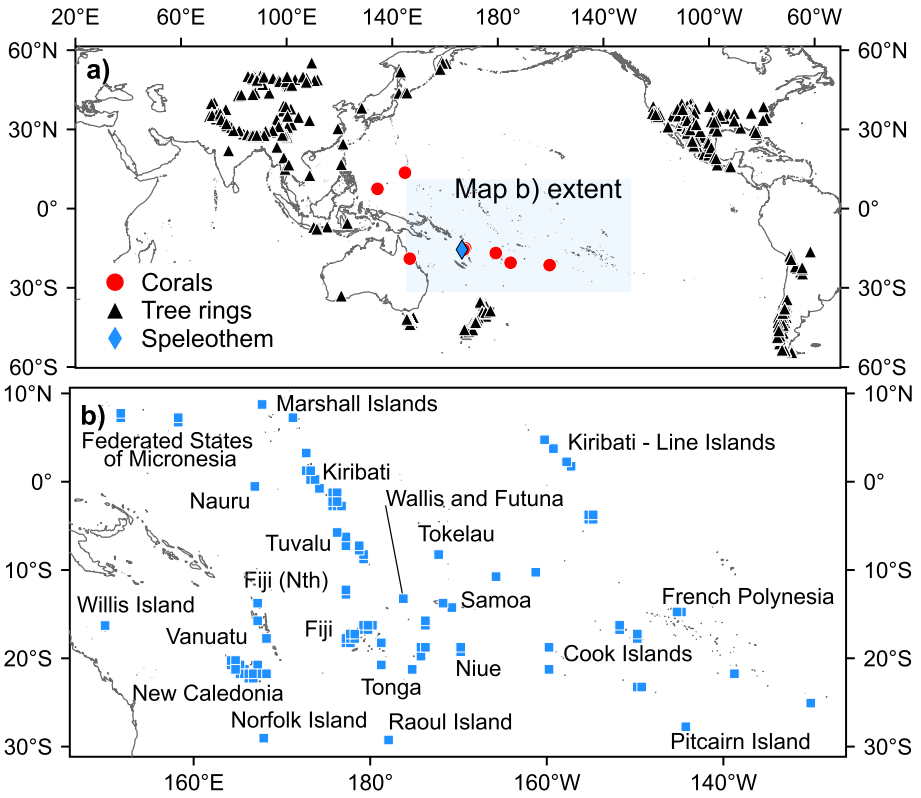

Fig. 1 **a** Locations of all proxy records included in one or more reconstructions, and **b** the grid point reconstruction targets for each island group

were seasonally averaged, while composite records (i.e. derived from multiple cores) were annually averaged.

Due to the small number of suitable in situ records, additional terrestrial proxies were selected from regions with strong teleconnections to the South Pacific. Tree-ring chronologies were selected from locations bordering the South Pacific rim with strong ENSO teleconnections. Approximately 670 chronologies previously used in the development of the Monsoon Asia Drought Atlas (Cook et al. 2010a, b), Eastern Australia and New Zealand Drought Atlas (Palmer et al. 2015), Mexican Drought Atlas (Stahle et al. 2016), and South American Drought Atlas (Morales et al. 2020) were downloaded from the International Tree-Ring Data Bank. The raw wood properties were standardised (i.e. detrended and transformed into dimensionless growth indices) using methods that preserve medium-term (multi-decadal) variability, including the 'signal-free' method (Wilson et al. 2019).

2.3 Reconstruction method

As this study targets ENSO-related droughts, we reconstructed the 6-month SPEI for the Southwest Pacific wet (November–April) season. Consistent with previously published drought atlases, SPEI was reconstructed using point-by-point regression (Cook et al. 2010a, 1999, 2007), a nested, principal components-based regression method. Using this method, regressive models are sequentially applied to the principal components (PCs) of the proxy network during a common calibration period between the predictors (proxies) and the predictands (SPEI data points). Only proxies with a significant relationship ($p \leq 0.1$; Spearman, Pearson, and robust Pearson) with the target data point were included in the predictor pool (Fig. 1, Figure S2). Each successive group of chronologies (nest) includes fewer chronologies but extends further back in time and is individually calibrated and verified against the instrumental data. We excluded any nest (and preceding nests) with a correlation of less than 0.4 with the most recent, best-replicated nest. The variance of the final reconstruction was stabilised using a 300-year spline to correct variance effects related to decreasing sample size back in time (Esper et al. 2002; Frank et al. 2006; Osborn et al. 1997).

In contrast to previous studies, a consistent calibration interval was not used for all SPEI data points. The last year of the calibration period was limited to 1998, a constraint imposed by the end date of many tree-ring chronologies. Based on climate data availability, the initial calibration year was then selected on an island group basis to maximise the calibration interval length. Between 38 and 57 years were used for calibration (Table S2). The available data for most island groups is too short to undertake split-period calibration and verification, which is the standard for dendrochronological reconstructions. Therefore, the reconstructions were primarily validated using a leave-one-out cross-validation procedure (Morales et al. 2020), using the cross-validation reduction of error (Meko 1997) as the validation statistic. A reconstruction point was considered valid with CVRE > 0.2. The CVRE is a relatively easy calibration target to pass and selecting predictors using correlation to the instrumental data may lead to an inflation of this statistic. Therefore, independent verification was undertaken for those stations with a sufficiently long data record, and the more stringent verification statistics, reduction of error (VRE), and coefficient of efficiency (VCE) were calculated.

To further verify the reconstruction results, we compared the SPaDA to previously published paleoclimate reconstructions of South Pacific climate variability (Table S3), which target ENSO indices derived from sea surface temperatures (SSTs). As all paleo-reconstructions contain large uncertainties, multiple comparisons were made to develop the best

possible picture of SST anomalies. Each of the ENSO reconstructions uses a different suite of proxy records, different reconstruction methods and seasonal targets, and has been rigorously calibrated and verified. There are, however, varying degrees of overlap in the proxy suite between the SPaDA and each of the reconstructions, so some similarity is expected.

2.4 Identifying extreme events

Extreme ENSO events are infrequent and cause abnormal drought patterns over the Pacific Islands, making them suitable targets for anomaly detection. To identify extreme events in the reconstruction, we used an 'Isolation Forest', an unsupervised machine learning algorithm that isolates outliers based on their anomalous characteristics (Liu et al. 2008). The algorithm has been successfully applied to detect anomalous patterns in published drought atlases (Marvel & Cook 2022). In an Isolation Forest, features are split along branches of a decision tree until each data point is isolated. More feature splits (branches) are required to isolate 'normal' data points compared to anomalous data points, providing the basis for anomaly detection. The results are quite sensitive to the user-defined 'contamination factor', which is the expected proportion of outliers in the training data set. We selected a contamination factor of 0.08, the best estimate of the proportion of extreme ENSO events since 1875 (see Text S1). The sensitivity of the analysis to this parameter is discussed in Text S2.

We only trained the algorithm over the instrumental period, when SST data is available to estimate the occurrence of extremes, because there is no reason to assume that the rate of occurrence (and thus the contamination factor) is stable through time. We then applied the trained model to the pre-1875 period. To account for uncertainty in the reconstructed SPEI on anomaly detection, 300 maximum entropy bootstrap replications (Vinod & López-de-Lacalle 2009) of reconstructed SPEI at each grid point were used to independently train the isolation forest on the post-1875 data and detect anomalies in the pre-1875 data. The hit rate of each anomalous year was then used as an estimate of the probability, with only those years with a greater than 0.5 hit rate designated as anomalous.

3 Reconstruction results

3.1 Calibration and validation

The fraction of instrumental variance explained is above 39% for all 102 grid points, above 50% for 91 grid points, and above 70% for 44 grid points. The reconstruction explains the most variance in SPEI for Kiribati and Tonga, and the least variance in SPEI for Norfolk Island, New Caledonia, and Tuvalu (Figure S3). Using the CVRE threshold of 0.2, the reconstruction extends back to 1410 CE for all grid points. Verification statistics for individual island grid points with suitable long-term records show that the model has reconstruction skill at 12 of the 13 gauges, as indicated by VRE and VCE values greater than 0 in the last, best-replicated nest (Table S4). Moving back in time, the reconstruction is considered valid for all nests with VRE and VCE greater than 0. The reconstruction period varies considerably across the verification points, with the first year of validity ranging between 0 and 1640 CE (Table S4). We therefore conservatively limit analysis to the period 1640–1998 CE. While uncertainty increases back in time across the entire domain, for some island groups the SPEI reconstruction is valid for several centuries prior to 1640 CE.

3.2 Drought anomalies during instrumental ENSO events

The spatial pattern of alternating wet/dry conditions between the western and eastern Pacific Islands is accurately captured by the SPaDA (Figure S4), with a large proportion of grid points severely dry (SPEI < −1) and severely wet (SPEI > 1) in the same year. The wavelet spectra (Torrence & Compo 1998) for the first principal component (PC1), which explains 56% of reconstruction variance, shows power concentrated in the ENSO band (2–8 years). Multi-taper method (MTM) spectral analysis (Mann & Lees 1996) indicates that the peak at 3–4 years is significant at the 99% level. The correlation between PC1 and the December-February Niño-34 index over the 1875–1998 CE period is −0.80 ($p < 0.001$). The second PC (PC2) explains ~7% of instrumental variance and shows significant power in the ENSO and decadal to multi-decadal frequency range. MTM analysis (Figure S5) identified a significant peak at ~24 years (99% level). Variability on multi-decadal timescales is expected in the reconstruction as the IPO influences drought in the Pacific Islands by shifting the mean position of the SPCZ (McGree et al. 2016).

We tested the ability of the SPaDA to reconstruct the Pacific Island drought response to warm and cold ENSO events using composite analysis. Figure 2 compares the average anomalies in the instrumental and reconstructed SPEI during the El Niño and La Niña events that occurred during the data period—1950–2000 CE for instrumental SPEI, and 1875–1998 CE for reconstructed SPEI. Two extreme event years falling within the calibration (i.e. overlapping) period, the 1997/1998 El Niño and 1988/1989 La Niña, are also compared. Reconstructed drought conditions in the SPaDA capture both the magnitude and spatial pattern of instrumental SPEI during both warm and cold ENSO events. The SPaDA also replicates the selected calibration period extreme events, although SPEI anomalies are somewhat underestimated for the strong La Niña in 1988/1989.

Any changes in the SPaDA-SST relationship could indicate non-stationary teleconnections between the South Pacific and the predictor regions, which would affect conclusions drawn from the SPaDA results. The stability of the relationship between drought in the SPaDA and SSTs was tested by calculating the 50-year running Pearson correlation between the PC1 of the reconstruction and the Niño-34 index (Fig. 2(i)). The relationship is stationary, as indicated by correlations remaining within the 95% confidence interval calculated from 1000 synthetic reconstructions with the same statistical characteristics as the SPaDA (Gallant et al. 2013). However, the relationship with Niño-34 is not stable for all grid points, e.g. Northern Vanuatu (Figure S6). This is most likely due to weaker reconstruction validity at these grid points rather than a genuine change in the strength of the relationship.

3.3 Comparison to other reconstructions

As ENSO is the primary mode of climatic variability influencing Pacific Island drought on interannual time scales, PC1 of the SPaDA is primarily an ENSO signal. We can therefore test the validity of the SPaDA by comparing PC1 to previously published ENSO reconstructions (Table S3). The running 50-year Pearson correlations between PC1 and five ENSO reconstructions over the common reconstruction interval are shown in Fig. 3. There is a high degree of fidelity between the results of this study and the tree-ring and multi-proxy ENSO reconstructions (Fig. 3(a)). Despite the overlap in predictor sets (notably the SPaDA and LI13 and the SPaDA and Z22m), the strength and stability of the correlations are quite

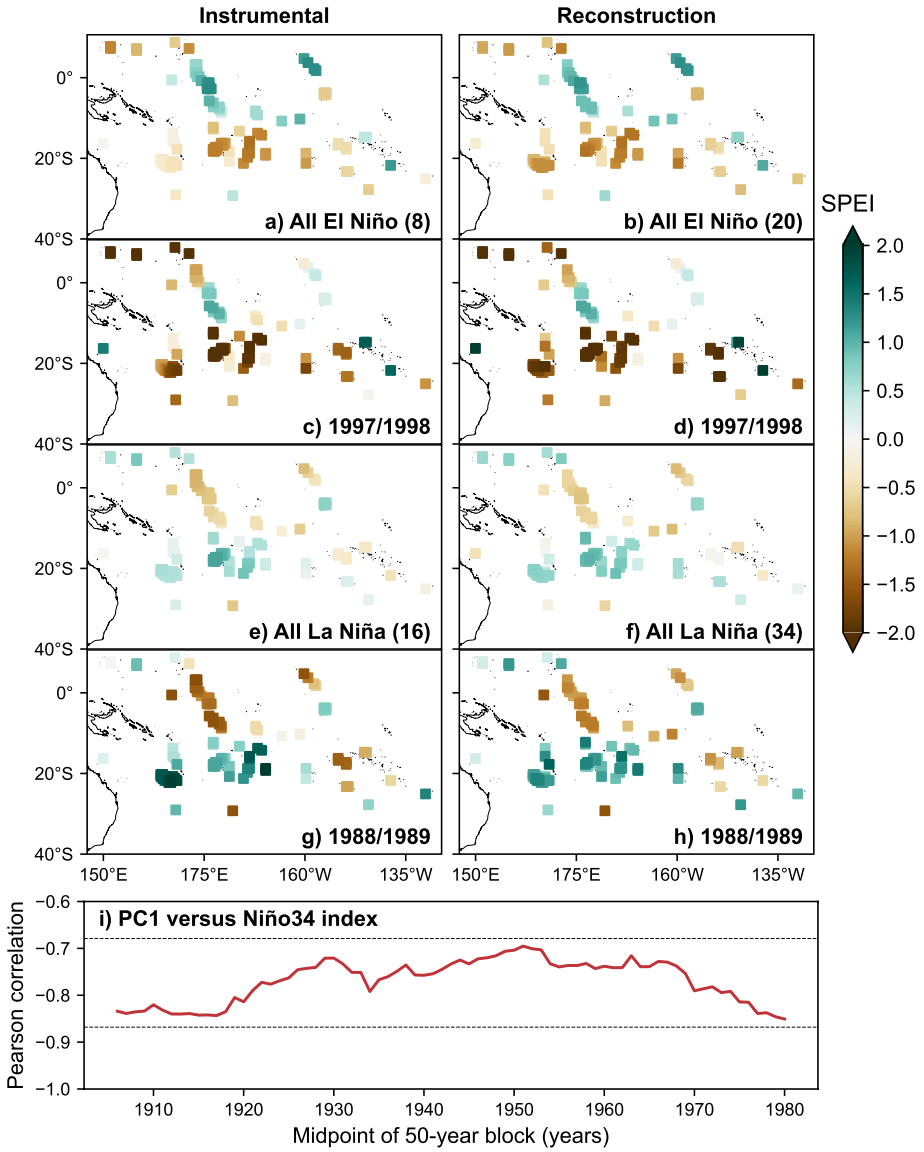

Fig. 2 Instrumental (left) versus reconstructed (right) November–April SPEI during El Niño and La Niña events over the data period (1950–2000 for instrumental, 1875–1998 for reconstruction). **a**, **b** All El Niño events; **c**, **d** the extreme El Niño of 1997/1998; **e**, **f** all La Niña events; **g**, **h** the extreme La Niña of 1989/1990. **i** 50-year running Pearson correlation between SPaDA PC1 and the December-February Niño-34 index with the 95% confidence interval calculated from synthetic data (dashed lines)

remarkable considering the SPaDA is a spatially resolved drought reconstruction calibrated only to post-1940 data. We observe no fading in the correlation strength before the SPaDA calibration period, and only minor fading prior to the calibration period of the other reconstructions. In contrast, PC1 and Z22c lose fidelity before 1850, with non-significant correlations during much of the first half of the common reconstruction interval (Fig. 3(b)).

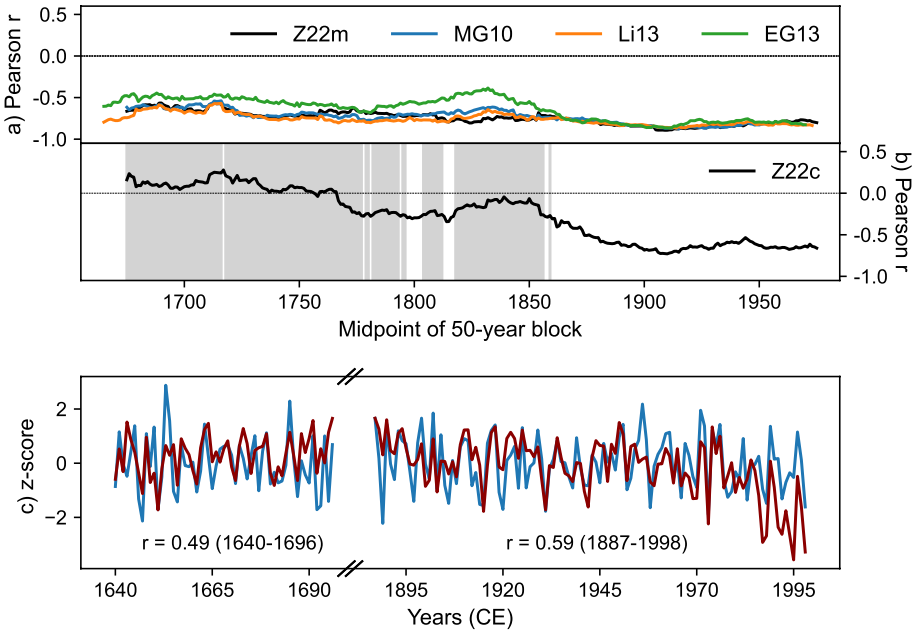

Fig. 3 Fifty-year running Pearson correlation between the SPaDA PC1 and the ENSO reconstructions **a** MG10: McGregor et al. (2010) multi-proxy reconstruction over 1650–1977 CE, LI13: Li et al. (2013) tree-ring reconstruction over the period 1640–1998 CE, EG13: Emile-Geay et al. (2013) multi-proxy reconstruction over 1640–1995, Z22m: Zhu et al. (2022) multi-proxy reconstruction over 1650–1998; **b** Z22c: Zhu et al. (2022) coral reconstruction over 1650–1998. Grey shading indicates correlations that are not significant ($p > 0.05$). **c** Comparison of the SPaDA PC1 (blue) with the Palmyra coral $\delta^{18}O$ series (red) for non-continuous segments over the SPaDA reconstruction interval. Both records were converted to z-scores for visualisation purposes

While coral proxies are located close to the geographical centre of ENSO action and are therefore the best recorders of direct ENSO (SST) impacts, they have several disadvantages including short length, discontinuities, and dating uncertainty, which is non-trivial for fossil coral records (DeLong et al. 2013; Zhu et al. 2022). The longest and most complete coral ENSO record published to date is located at Palmyra atoll, covering 535 of the past 1000 years in one modern and two fossil coral segments (Cobb et al. 2003). Li et al. (2013) found significant correlations between their tree-ring-based ENSO reconstruction and the Palmyra fossil record by adjusting the coral Uranium/Thorium dates within the analytical error windows. Making the same adjustment to the Palmyra fossil segment dates, we also find significant correlations between SPaDA PC1 and the Palmyra record over the last 350 years (Fig. 3(c)). As the SPaDA and the Palmyra record are entirely independent, the fidelity with this record provides substantial confidence in the robustness of the SPaDA over the reconstruction period. The coral-based reconstruction Z22c (Fig. 3(b)) is highly correlated to both the modern and fossil portions of the Palmyra record (Pearson correlation > -0.90) and has little interannual variance during periods when Palmyra observations are unavailable (Zhu et al. 2022). The low variance in Z22c in the period when the Palmyra record is unavailable and dating uncertainty in the fossil portion of the Palmyra record could thus explain the loss of correlation between Z22c and the SPaDA in the early part of the common reconstruction interval.

3.4 Reconstructed SPEI during historical drought events

Figure 4 shows reconstructed SPEI for four historical drought events. The 'Year of Hunger' was a series of droughts and unseasonable frosts which occurred over 1785–1787 in Mexico, resulting in famine and the estimated deaths of 300,000 people (Therrell 2005). Tree-ring reconstructions have shown that the drought pattern in central America was consistent with the influence of La Niña (Therrell 2005). Reconstructed SPEI shows dry conditions over the eastern and equatorial Pacific, and wet conditions in the southwest Pacific, consistent with La Niña conditions during this period (Fig. 4(a)).

Historical records (Russell 1877) describe a severe drought experienced by European colonialists within 2 years of arriving in Sydney, Australia. Tree-ring reconstructions indicate that drought conditions were experienced across eastern Australia during the 'Settlement Drought' of 1791–1795, with the most extreme soil moisture deficits occurring in the summer of 1791/1792 (Palmer et al. 2015). Simultaneously, drought and famine occurred over much of India and the Caribbean (Grove 2007). Paleoclimate records suggest the Australian Settlement Drought was associated with an unusually strong El Niño (Gergis & Fowler 2009). No documentary evidence is available to confirm whether this event also caused anomalous rainfall over the Pacific Islands; however, SPEI anomalies during 1791/1792 are amongst the highest during the reconstruction period. Based on the SPaDA reconstruction, an extreme drought occurred over much of the Southwest Pacific, with extreme wet conditions across the Equatorial Pacific (Fig. 4(b)).

Stalagmite isotopes from Espiritu Santo, Vanuatu, indicate an unusually dry year in 1866 ± 3 years (Partin et al. 2013). A drought occurring around 1866 or 1867 was also recorded in the diary of John G. Paton, who was a missionary on Aniwa, 500 km to the south (Paton 1893). The SPaDA shows localised drought conditions in the southernmost Vanuatu grid point during 1865/1866 (Fig. 4(c)). While nearby New Caledonia and Fiji

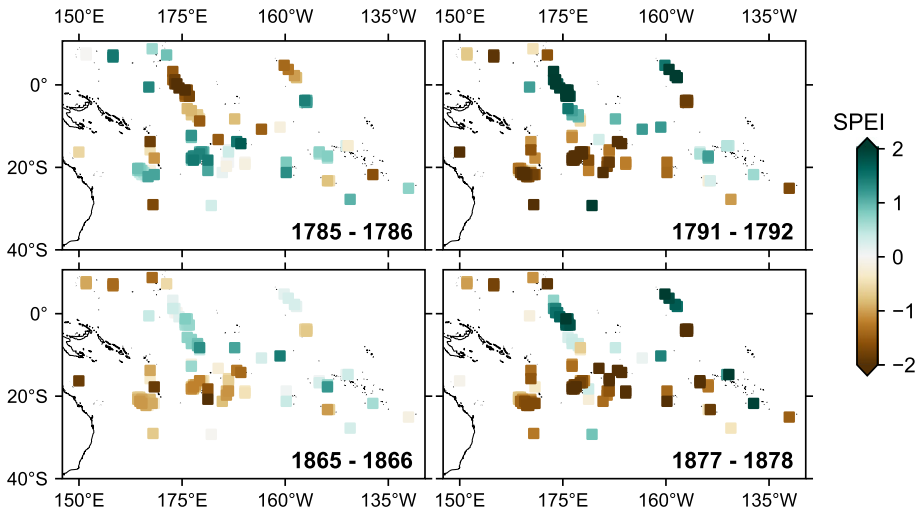

Fig. 4 November–April SPEI during known historical droughts: the Mexican Year of Hunger (1785–1786), the Australian Settlement Drought (1791–1793), the Vanuatu drought (1865–1866), and the Great Drought (1877–1878)

show only moderately dry conditions, SPEI anomalies indicate severe drought in the preceding year (Figure S7). The SPaDA suggests that the Vanuatu drought began in the summer of 1864/1865, persisted over 1865, and weakened in the autumn of 1866.

The Great Drought (1876–1878) was a concurrent period of multiyear droughts across Monsoon Asia, Brazil, Africa, and the Pacific. Widespread crop failures resulted in the 'Global Famine', with estimated fatalities exceeding 50 million people (Singh et al. 2018). In New Caledonia, a disastrous drought at the end of 1877 exacerbated tensions between the Melanesian Kanak peoples and the French colonial regime, with thousands of Kanak casualties (Davis, 2002). The yam crop in Fiji and the taro crop in Vanuatu—both staples—failed due to a lack of rainfall. In contrast, torrential rain damaged crops in Kiribati leading to starvation deaths on the Gilbert Group islands (D'Aubert & Nunn, 2012). The Great Drought is attributed to an El Niño of extreme strength and duration coinciding with a record positive Indian Ocean Dipole event (Singh et al. 2018). The SPaDA shows anomalously dry conditions over much of the southwest Pacific from 1877 to 1878, with extreme drought occurring in Fiji, Niue, Tonga, and the Cook Islands and unusual wet conditions in Kiribati, the Line Islands, and parts of French Polynesia (Fig. 4(d)).

The selected historical cases demonstrate that the SPaDA provides reliable spatiotemporal information on drought events outside of the instrumental period. Identifying droughts in the SPaDA for which significant documentary or other non-tree ring evidence is available (i.e. the Australian Settlement Drought, the Great Drought) greatly increases the confidence in the results. It is also promising that the SPaDA appears to capture localised drought events, which may be related to climate patterns other than ENSO. Verification against independent records shows that the SPaDA has the potential to contribute to our knowledge of climate extremes in the South Pacific.

4 Analysis and discussion

4.1 Identification of extreme events

Anomalous hydroclimatic states in the SPaDA were identified using an Isolation Forest algorithm, with a contamination factor of 0.08, the best available estimate of the occurrence of extreme La Niña and El Niño events since 1875. Figure 5 shows the 32 outliers identified as anomalous in > 50% of bootstrap replications, 18 of which show El Niño–like drought patterns and 14 La Niña–like drought patterns. These years are highlighted as circles on the SPaDA PC1, scaled to match the instrumental Niño-34 index. All but one of the outliers are classified as strong ENSO events, defined by values above or below 1.5 standard deviations from the PC1 mean. The remaining anomalous year (1983) lies very close to the threshold. Thus, the Isolation Forest identifies years with unusually large SPEI values consistent with enhanced SST anomalies and not patterns associated with more localised drought features. The algorithm cannot attribute spatial anomalies to specific internal variability or external forcing modes. We therefore classified the anomalous states as 'El Niño–like drought' or 'La Niña–like drought' based on their similarity to the standard patterns of drought over the South Pacific during ENSO phases. Despite this, spatial drought patterns consistent with instrumental ENSO events and appearing as points over the 1.5 standard deviation threshold of PC1 values strongly suggest that a significant ENSO event occurred.

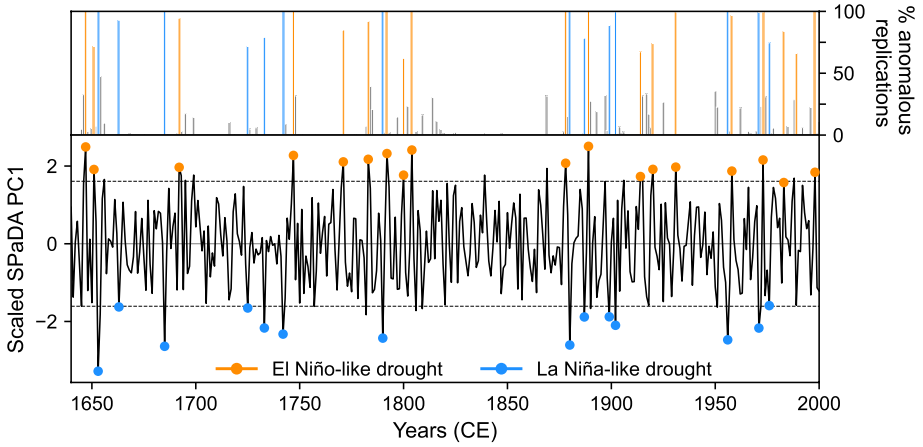

Fig. 5 SPaDA PC1 scaled to the instrumental Niño-34 index with the 18 El Niño–like drought (orange circles) and 14 La Niña–like drought anomalies (blue circles). Dashed horizontal lines indicate ± 1.5 standard deviation threshold for strong ENSO events. The percentage of MEboot replications of reconstructed SPEI in which an anomalous state was identified (orange and blue bars, top panel) provides an estimate of the impact of reconstruction uncertainty on the results. Grey bars show years identified as anomalous in less than 50% of replications using a contamination factor of 0.08 (top panel)

4.2 Reconstructed SPEI during anomalous years

Six of the seven La Niña–like drought years identified since 1875, the period when SST observations are available, correspond to La Niña events (Figure S8). None of the three largest La Niña–like drought outliers occurred in the twentieth century; the most anomalous spatial drought pattern is 1880, followed by 1653, which shows the most extreme PC1 values, and 1685. The SPaDA results suggest that in previous centuries, drought episodes resulting from La Niña events have exceeded the magnitude of the instrumental period events. However, for La Niña–like drought events, anomaly detection provides little additional information beyond a simple threshold applied to the SPaDA PC1. The amplitude of PC1 negative anomalies (our proxy for the Niño-34 index) is thus sufficient to describe the strength of the La Niña–like drought outlier events. This is consistent with studies based on instrumental datasets, which find a single SST index is adequate to measure the strength of La Niña events (Cai et al. 2015).

Figure 6 shows SPEI for the 18 El Niño–like anomalous years. Eight of the nine outliers identified since 1875 correspond to El Niño events. Both the Australian Settlement Drought (1792) and the Great Drought (1878), droughts with documentary evidence that suggests global impact, are identified as years of unusual hydroclimatic activity. For El Niño–like drought outliers, the Isolation Forest identifies anomalous characteristics in drought patterns beyond just the magnitude of the SPEI anomalies. The largest El Niño–like drought outlier is 1997/1998, although the SPaDA PC1 value for this year is exceeded in 14 other anomalous years. The algorithm also identifies 1982/1983 as an outlier, although it does not exceed the 1.5 standard deviation threshold for strong ENSO events. Eight other years, not identified as outliers, do exceed this threshold.

Unlike strong La Niña events, strong El Niño events show non-linear characteristics that are not easily described using a single ENSO index. There are two distinct types of El Niño phases, differentiated by larger SST anomalies towards the eastern or central Pacific, usually referred to as the East Pacific/canonical El Niño and the Central Pacific/El Niño

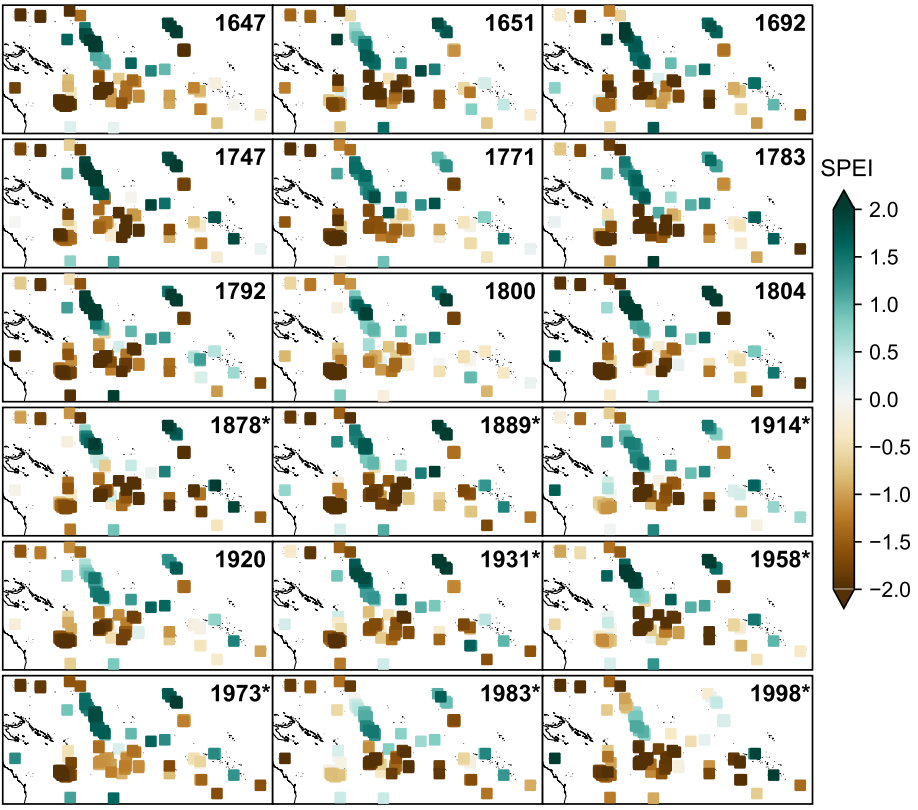

Fig. 6 El Niño–like drought patterns during the 18 years identified as outliers. Starred years (*) are historical El Niño events (1973, 1983, and 1998 are the three instrumental-period extreme El Niño events where the SPCZ took a zonal orientation)

Modoki, respectively (Wiedermann et al. 2021; Yeh et al. 2014). These phases are associated with distinct patterns of rainfall across the Pacific islands (Murphy et al. 2014) and certain regions of the globe (Taschetto et al. 2010) due to SST-driven modifications of atmospheric circulation patterns (Wiedermann et al. 2021).

The 1982/1983 and 1997/1998 El Niño events, in particular, exhibited SST and precipitation characteristics distinct from any other warm ENSO event. Exceptionally warm SST anomalies peaked towards the eastern Pacific, weakening the east–west SST gradients, strengthening the ITCZ in the eastern equatorial Pacific region and allowing the SPCZ to shift by up to ten degrees of latitude towards the equator, achieving a near-zonal orientation (Cai et al. 2012; Santoso et al. 2017). Rainfall non-linearity resulting from the shift in the convergence zones, particularly increased precipitation in the usually dry eastern equatorial Pacific (Niño3 region, east of 120°W), has been used to identify the occurrence of similar zonal El Niño events in climate models (Cai et al. 2014).

Here, we investigate whether the Isolation Forest identifies spatial drought anomalies consistent with extreme El Niño events in the SPaDA. The spatial coverage of the SPaDA was determined by the location of Pacific Islands with sufficient meteorological data, which thus does not extend to the eastern equatorial Pacific region. During very strong El Niño events, substantial precipitation anomalies can be observed in the SPaDA region as

increased precipitation along the equator to the east of the Solomon Islands, and decreased precipitation throughout the southwest Pacific and to the north of the Equator. The shift in orientation and increase in convergence zone intensity results in more extreme precipitation anomalies than other El Niño years for most Pacific Islands and precipitation anomalies of the opposite sign to other years in some locations (Murphy et al. 2014).

Murphy et al. (2014) identified six Pacific Islands which show different characteristics during extreme El Niño events compared to other El Niño events. For Majuro, the Marshall Islands, shifts in the ITCZ result in generally wet La Niña and dry El Niño events, with much larger dry anomalies during extreme El Niño events. ENSO signals of opposite sign are experienced by the northern and southern Cook Islands, with El Niño events wet in the north and dry in the south. The northward movement of the SPCZ that resulted in the wettest year on record for Penrhyn, northern Cook Islands, in 1982/1983 and 1997/1998 was the driest on record for Rarotonga, southern Cook Islands. Funafuti, Tuvalu, is in the transition zone between these wet and dry El Niño regions and experiences mixed precipitation signals between ENSO phases. Funafuti had its wettest years on record during 1982/1983 and 1997/1998. Tarawa, Kiribati, and Nauru in the western Equatorial Pacific have enhanced rainfall during El Niño events and suppressed rainfall during La Niña events. However, extreme El Niño events resulted in opposite precipitation signals (dry rather than wet El Niño).

Figure 7 shows SPEI during the 18 El Niño–like drought outliers identified by the Isolation Forest for these six islands compared to average SPEI during El Niño and La Niña events. More than 80% (15/18) of outlier years show characteristics consistent with instrumental precipitation anomalies during zonal SPCZ events at one or more stations (starred years). The SPaDA more readily identifies atypical characteristics at stations with

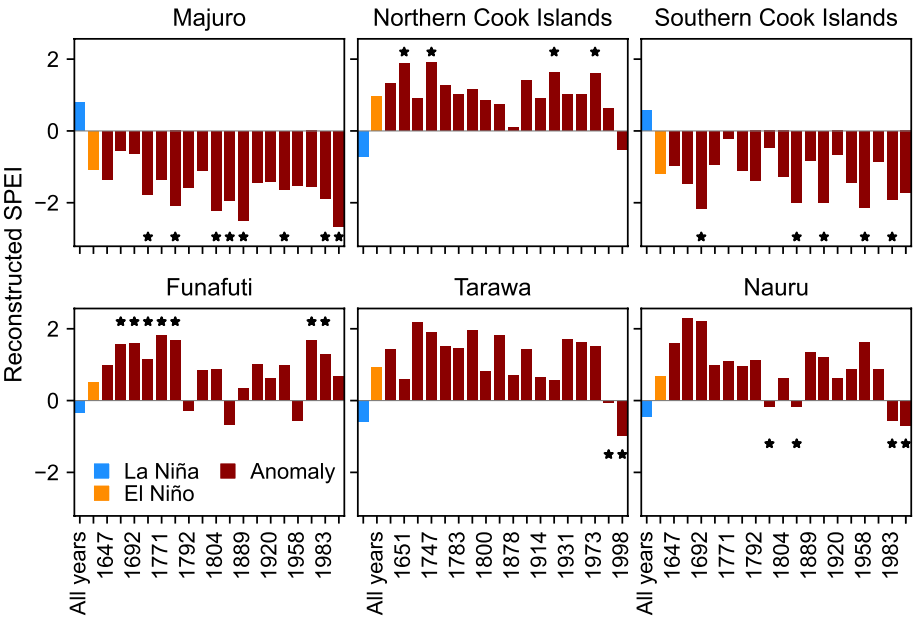

Fig. 7 November–April SPEI for six Pacific Islands in all years identified as El Niño–like drought anomalies (red), compared to average SPEI in La Niña years (blue) and El Niño years (orange). Starred years show drought characteristics consistent with instrumental precipitation during extreme El Niño events when the SPCZ took a zonal orientation

enhanced precipitation anomalies compared to Nauru and Tarawa which demonstrate 'sign switching'. Only 2 years outside of the calibration period are consistent with a zonal SPCZ in the Nauru reconstruction, and no pre-calibration period years are atypical in the Tarawa reconstruction. This result is likely impacted by our use of a linear model to reconstruct the strongly non-linear relationship to precipitation during extreme El Niño events at these stations and the small number of such events during the calibration period.

Not all extreme El Niño events co-occur with a zonal SPCZ. The most recent extreme El Niño, which occurred in 2015/2016 (outside our reconstruction period), had record-breaking warm SST anomalies in the central Pacific but weaker shifts in the ITCZ and SPCZ than other extreme events (Santoso et al. 2017). Based on the SPEI magnitude and documentary evidence of global impact, 1646/1647 and 1791/1792 may still be classified as extreme El Niño events despite lacking atypical drought patterns that suggest a zonal SPCZ (Figs. 6 and 7).

4.3 No trend in anomalous South Pacific droughts

Our results show that La Niña– and El Niño–like drought patterns of equal or greater magnitude than those of the instrumental period have occurred semi-regularly over the Southwest Pacific in the last 350 years. A greater frequency of anomalous events is observed in the recent (training) interval compared to the pre-instrumental data, increasing from an average of 1 every 14.6 years (1640–1874) to 1 every 7.8 years (1875–1998). However, the trend of increasing anomalous events is not statistically significant (Cox-Lewis test, $p > 0.05$), regardless of whether the Isolation Forest or the simple threshold method was used to identify outliers. We therefore cannot reject the null hypothesis—that the occurrence of extreme/anomalous hydroclimatic states has remained stable over the reconstruction interval.

Anthropogenic climate change is projected to increase the frequency of zonal SPCZ events due to enhanced warming of the eastern Equatorial Pacific (Cai et al. 2012). Other studies suggest that recent El Niño extremes are more intense than in the past (Freund et al. 2019) and that human influence may already be contributing to an increased likelihood for zonal SPCZ occurrence (Power et al. 2017). Despite this, we cannot yet find statistical evidence of increased drought-event frequency consistent with a zonal SPCZ orientation in the later twentieth century. The anomalous drought patterns indicate that the co-occurrence of strong El Niño events and zonal SPCZ orientation observed during the 1982/1983 and 1997/1998 events is present throughout the reconstruction interval.

Linsley et al. (2017) similarly found no trend in the number of zonal SPCZ events identified in their coral record from the western Equatorial Pacific (not used to develop the SPaDA). Nevertheless, there are several constraints on the SPaDA that may hamper the identification of trends. Robust meteorological data is not available for all islands in the last decade of the reconstruction, which may contribute to the underestimation of SPEI anomalies for recent events such as 1988/1989, and there is insufficient instrumental data coverage over the SPaDA domain to assess trends in extremes since 2000. In addition, the linear (principal components) method may not be suitable for reconstructing strongly non-linear rainfall trends at some stations, underestimating the occurrence of zonal events. There is evidence that while climate change may increase the spatial extent of ENSO teleconnections, the existing teleconnections may not be simply strengthened (Perry et al. 2017). Reconstructions based predominantly on predictors from teleconnected regions, like the SPaDA, may therefore not identify all changes to ENSO. Finally, the substantial interannual and multidecadal variability in the South Pacific likely dominates any signal from anthropogenic warming (Brown et al. 2020).

5 Conclusions

We developed the first spatially resolved multi-proxy drought reconstruction for the South Pacific islands. The SPaDA provides a 350-year dataset of South Pacific drought for comparison with other proxy records, documentary data, and climate model outputs. The reconstruction integrates coral proxies, which provide local information on the South Pacific hydroclimate but are limited in number and length, with a network of tree rings targeting Pacific climate variability through remote teleconnections. The reconstruction demonstrates the benefits of multiproxy reconstructions incorporating tree rings, which allow for the alignment of other proxy records without chronological error.

The SPaDA closes the gap between existing paleo-reconstructions of point ENSO indices, and a spatially resolved drought atlas, allowing both the hydroclimate of individual islands and regional patterns of drought to be assessed. While contrasting east/west South Pacific drought anomalies are a consistent feature of the SPaDA, the precise pattern of drought varies between each ENSO event (Figs. 2, 6, S8). The benefit of a spatially resolved dataset to assess the impacts of ENSO events on small Pacific islands is highlighted in the case of El Niño extremes, which can have substantially different climatic impacts than more moderate events (Fig. 6). The SPaDA may also prove useful to assess the past occurrence of canonical and El Niño Modoki events, which show distinct precipitation patterns over the Pacific.

Climate models suggest that the frequency of extreme El Niño events will increase in future. This would substantially impact the South Pacific islands under the influence of the SPCZ, with an increase in severe flooding, drought, or anomalous precipitation patterns in many locations. To understand future vulnerabilities and adapt to projected climate change impacts on water resources, robust estimates of the likelihood of extreme events are required. The SPaDA shows that extreme El Niño events characterised by very strong southwest Pacific drought anomalies and a zonal SPCZ orientation have occurred since 1640 CE, prior to an anthropogenic global warming signal. The SPaDA thus provides a valuable baseline of, and multi-centennial context for, the occurrence of ENSO extremes in the instrumental period. The reconstruction helps improve our understanding of past hydroclimate variability in the southwest Pacific and can be used to evaluate the performance of climate models for Pacific Island countries.

Supplementary Information The online version contains supplementary material available at https://doi.org/10.1007/s10584-023-03585-2.

Acknowledgements The authors thank the following agencies for the provision of climate data to support this research: Fiji Meteorological Service, Météo-France Regional Service New Caledonia, Wallis and Futuna, Nauru National Meteorology Service, the Meteorological Service of New Zealand, and the Australian Bureau of Meteorology.

Author contributions All authors contributed to the study conception and design. Curation of the tree-ring dataset was undertaken by Jonathan Palmer. All other data preparation, coding, and analysis were performed by Philippa Higgins. The first draft of the manuscript was written by Philippa Higgins and all authors commented on previous versions of the manuscript. All authors read and approved the final manuscript.

Funding Open Access funding enabled and organized by CAUL and its Member Institutions. This work was supported by the ARC Centre of Excellence in Australian Biodiversity and Heritage (grant no. CE170100015). Philippa Higgins was supported by an Australian Government Research Training Scholarship and the UNSW Scientia PhD Scholarship Scheme. Fiona Johnson was supported by the Australian Research Council Training Centre in Data and Analytics for Resources and Environments (DARE) IC190100031 and the UNSW Scientia Program.

Data Availability The instrumental and reconstructed November–April SPEI datasets generated during the current study are available in the Zenodo repository at https://doi.org/10.5281/zenodo.7425832. The

instrumental Niño-34 index was downloaded from the NOAA ESRL Physical Sciences Laboratory at https://psl.noaa.gov/gcos_wgsp/Timeseries/Nino34/. All ENSO reconstructions and the Palmyra coral record were downloaded from the NOAA/World Data Service for Paleoclimatology archive at https://www.ncei.noaa.gov/access/paleo-search/, except for the Zhu et al. (2022) reconstructions which were downloaded from the Zenodo repository at 105281/zenodo.5716165.

Declarations

Competing interests The authors declare no competing interests.

References

Annamalai H, Keener V, Widlansky MJ, & Hafner J (2015) El Niño strengthens in the Pacific: preparing for the impacts of drought. Asia Pacific Issues, 2015(122).

Beguería S, Sergio M, Vicente-Serrano FR, Latorre B (2014) Standardized precipitation evapotranspiration index (SPEI) revisited: parameter fitting, evapotranspiration models, tools, datasets and drought monitoring. Int J Climatol 34(10):3001–3023. https://doi.org/10.1002/joc.3887

Brázdil R, Kiss A, Luterbache J, Nash DJ, Řezníčková L (2018) Documentary data and the study of past droughts: a global state of the art. Climate Past 14(12):1915–1960. https://doi.org/10.5194/cp-14-1915-2018

Brown JR, Lengaigne M, Lintner BR, Widlansky MJ, van der Wiel K, Dutheil C, Linsley BK, Matthews AJ, Renwick J (2020) South Pacific Convergence Zone dynamics, variability and impacts in a changing climate. Nat Rev Earth Environ 1(10):530–543. https://doi.org/10.1038/s43017-020-0078-2

Cai W, Lengaigne M, Borlace S, Collins M, Cowan T, McPhaden MJ, Timmermann A, Power S, Brown J, Menkes C, Ngari A, Vincent EM, Widlansky MJ (2012) More extreme swings of the South Pacific convergence zone due to greenhouse warming. Nature 488(7411):365–369. https://doi.org/10.1038/nature11358

Cai W, Borlace S, Lengaigne M, van Rensch P, Collins M, Vecchi G, Timmermann A, Santoso A, McPhaden MJ, Wu L, England MH, Wang G, Guilyardi E, Jin F-F (2014) Increasing frequency of extreme El Niño events due to greenhouse warming. Nat Clim Chang 4(2):111–116. https://doi.org/10.1038/nclimate2100

Cai W, Wang G, Santoso A, Mcphaden MJ, Wu L, Jin FF, Timmermann A, Collins M, Vecchi G, Lengaigne M, England MH, Dommenget D, Takahashi K, Guilyardi E (2015) Increased frequency of extreme La Niña events under greenhouse warming. Nat Clim Chang 5(2):132–137. https://doi.org/10.1038/nclimate2492

Capotondi A, Wittenberg AT, Newman M, Di Lorenzo E, Yu JY, Braconnot P, Cole J, Dewitte B, Giese B, Guilyardi E, Jin FF, Karnauskas K, Kirtman B, Lee T, Schneider N, Xue Y, Yeh SW (2015) Understanding ENSO diversity. Bull Am Meteor Soc 96(6):921–938. https://doi.org/10.1175/BAMS-D-13-00117.1

Cobb KM, Charles CD, Cheng H, Edwards RL (2003) El Niño/Southern Oscillation and tropical Pacific climate during the last millennium. Nature 424(6946):271–276. https://doi.org/10.1038/nature01779

Cook ER, Meko DM, Stahle DW, Cleaveland MK (1999) Drought reconstructions for the continental United States. J Clim 12(4):1145–1163. https://doi.org/10.1175/1520-0442(1999)012%3c1145:drftcu%3e2.0.co;2

Cook ER, Seager R, Cane MA, Stahle DW (2007) North American drought: reconstructions, causes, and consequences. Earth Sci Rev 81(1–2):93–134. https://doi.org/10.1016/j.earscirev.2006.12.002

Cook ER, Anchukaitis KJ, Buckley BM, D'Arrigo RD, Jacoby GC, Wright WE (2010a) Asian monsoon failure and megadrought during the last millennium. Science 328:486–489. https://doi.org/10.1126/science.1185188

Cook ER, Anchukaitis KJ, Buckley BM, D'Arrigo RD, Jacoby GC, Wright WE (2010b) Asian monsoon failure and megadrought during the last millennium: supporting Information. Science 328:486–489. https://doi.org/10.1126/science.1185188

Cook ER,Seager R, Kushnir Y, Briffa KR, Büntgen U, Frank D, Krusic PJ, Tegel W, Schrier GV, Andreu-Hayles L, Baillie M, Baittinger C, Bleicher N, Bonde N, Brown D, Carrer M, Cooper R, Eùfar K, DIttmar C,…Zang C (2015) Old World megadroughts and pluvials during the Common Era. Science Advances, 1(10), 1–10https://doi.org/10.1126/sciadv.1500561

Davis M (2002) Late Victorian holocausts: El Niño famines and the making of the third world. Verso Books, London. ISBN:9781781680612

DeLong KL, Quinn TM, Taylor FW, Shen C-C, Lin K (2013) Improving coral-based paleoclimate reconstructions by replicating 350 years of coral Sr/Ca variations. Palaeogeogr Palaeoclimatol Palaeoecol 373:6–24. https://doi.org/10.1016/j.palaeo.2012.08.019

Emile-Geay J, Cobb K, Mann M, Wittenberg A (2013) Estimating Central Equatorial Pacific SST Variability over the Past Millennium. Part II: Reconstructions and Implications. J Clim 26(7):2329–2352. https://doi.org/10.1175/JCLI-D-11-00511.1

Esper J, Cook ER, Schweingruber FH (2002) Low-frequency signals in long tree-ring chronologies for reconstructing past temperature variability. Science 295(5563):2250–2253. https://doi.org/10.1126/science.1066208

Frank D, Esper J, & Cook ER (2006) On variance adjustment in tree-ring chronology development. In H. H. Gärtner, M. Monbaron, & G. Schleser (Eds.), TRACE. Tree Rings in Archaeology, Climatology and Ecology. Volume 4. (pp. 56–66).

Freund MB, Henley BJ, Karoly DJ, McGregor HV, Abram NJ, Dommenget D (2019) Higher frequency of Central Pacific El Niño events in recent decades relative to past centuries. Nat Geosci 12(6):450–455. https://doi.org/10.1038/s41561-019-0353-3

Gallant AJE, Phipps SJ, Karoly DJ, Mullan AB, Lorrey AM (2013) Nonstationary Australasian teleconnections and implications for paleoclimate reconstructions. J Clim 26(22):8827–8849. https://doi.org/10.1175/JCLI-D-12-00338.1

Gergis JL, Fowler AM (2009) A history of ENSO events since A.D. 1525: implications for future climate change. Clim Chang 92(3–4):343–387. https://doi.org/10.1007/s10584-008-9476-z

Grove RH (2007) The Great El Niño of 1789–93 and its global consequences: reconstructing an extreme climate event in world environmental history. Mediev Hist J 10(1–2):75–98. https://doi.org/10.1177/097194580701000203

Harris I, Osborn TJ, Jones P, Lister D (2020) Version 4 of the CRU TS monthly high-resolution gridded multivariate climate dataset. Scientific Data 7(1):1–18. https://doi.org/10.1038/s41597-020-0453-3

Iese V, Kiem AS, Mariner A, Malsale P, Tofaeono T, Kirono DGC, Round V, Heady C, Tigona R, Veisa F, Posanau K, Aiono F, Haruhiru A, Daphne A, Vainikolo V, Iona N (2021) Historical and future drought impacts in the Pacific islands and atolls. Clim Change 166(1–2):1–24. https://doi.org/10.1007/s10584-021-03112-1

Johnson F, Higgins P, & Stephens C (2021) Climate change and hydrological risk in the Pacific: a Humanitarian Engineering perspective. Journal of Water and Climate Change, 1–32. https://doi.org/10.2166/wcc.2021.277

Li J, Xie S-P, Cook ER, Morales MS, Christie DA, Johnson NC, Chen F, D'Arrigo R, Fowler AM, Gou X, Fang K (2013) El Niño modulations over the past seven centuries. Nat Clim Chang 3(9):822–826. https://doi.org/10.1038/nclimate1936

Linsley BK, Wu HC, Rixen T, Charles CD, Gordon AL, Moore MD (2017) SPCZ zonal events and downstream influence on surface ocean conditions in the Indonesian Throughflow region. Geophys Res Lett 44(1):293–303. https://doi.org/10.1002/2016GL070985

Liu FT, Ming Ting K, & Zhou ZH (2008) Isolation forest. Eighth IEEE Int. Conf. on Data Mining, 413–422. https://doi.org/10.1109/ICDM.2008.17

Lorrey A, Dalu GI, Renwick J, Diamond H, Gaetani M (2012) Reconstructing the South Pacific Convergence Zone position during the presatellite era: a La Niña case study. Mon Weather Rev 140(11):3653–3668. https://doi.org/10.1175/MWR-D-11-00228.1

Lough JM, Lewis SE, Cantin NE (2015) Freshwater impacts in the central Great Barrier Reef: 1648–2011. Coral Reefs 34(3):739–751. https://doi.org/10.1007/s00338-015-1297-8

Ludert A, Wang B, Merrifield MA (2018) Characterization of dry conditions across the U.S.-Affiliated Pacific Islands during near-neutral ENSO phases. J Clim 31(16):6461–6480. https://doi.org/10.1175/JCLI-D-17-0561.1
Mann ME, Lees JM (1996) Robust estimation of background noise and signal detection in climatic time series. Clim Change 33(3):409–445. https://doi.org/10.1007/BF00142586
Marvel K, & Cook BI (2022) Using machine learning to identify novel hydroclimate states. Phil. Trans. R. Soc. A, 380. https://doi.org/10.1098/rsta.2021.0287
McGree S, Schreider S, Kuleshov Y (2016) Trends and variability in droughts in the Pacific islands and Northeast Australia. J Clim 29(23):8377–8397. https://doi.org/10.1175/JCLI-D-16-0332.1
McGregor S, Timmermann A, Timm O (2010) A unified proxy for ENSO and PDO variability since 1650. Clim Past 6(1):1–17. https://doi.org/10.5194/cp-6-1-2010
McPhaden MJ, Zebiak SE, & Glantz MH (2006) ENSO as an integrating concept in earth science. Science, 314. https://www.science.org
Meko DM (1997) Dendroclimatic reconstruction with time varying predictor subsets of tree indices. J Clim 10(4):687–696. https://doi.org/10.1175/1520-0442(1997)010%3c0687:DRWTVP%3e2.0.CO;2
Morales MS, Cook ER, Barichivich J, Christie DA, Matskovsky V, Aravena JC, Lara A, Mundo IA, Alvarez C, Lopez L, Luckman B, Lister D, Harris I, Philip D, Williams P, Velazquez G, Aliste D, Aguilera-betti I (2020) 600 years of South American tree rings reveal an increase in severe hydroclimatic events since mid-20th century. PNAS 117(29):16816–16823. https://doi.org/10.1073/pnas.2002411117
Murphy BF, Power SB, Mcgree S (2014) The varied impacts of El Niño-Southern Oscillation on Pacific Island climates. J Clim 27(11):4015–4036. https://doi.org/10.1175/JCLI-D-13-00130.1
Osborn TJ, Briffa KR, Jones PD (1997) Adjusting variance for sample-size in tree-ring chronologies and other regional mean time series. Dendrochronologia 15:89–99
Palmer JG, Cook ER, Turney CSM, Allen K, Fenwick P, Cook BI, O'Donnell A, Lough J, Grierson P, & Baker P (2015) Drought variability in the eastern Australia and New Zealand summer drought atlas (ANZDA, CE 1500–2012) modulated by the Interdecadal Pacific Oscillation. Environmental Research Letters, 10(12). https://doi.org/10.1088/1748-9326/10/12/124002
Partin JW, Quinn TM, Shen CC, Emile-Geay J, Taylor FW, Maupin CR, Lin K, Jackson CS, Banner JL, Sinclair DJ, Huh CA (2013) Multidecadal rainfall variability in South Pacific Convergence Zone as revealed by stalagmite geochemistry. Geology 41(11):1143–1146. https://doi.org/10.1130/G34718.1
Paton JG (1893) The Story of John G. Paton Told for Young Folks or Thirty Years among South Sea Cannibals. Hodder and Stoughton.
Perry SJ, McGregor S, Gupta AS, England MH (2017) Future changes to El Niño-Southern Oscillation temperature and precipitation teleconnections. Geophys Res Lett 44(20):10608–10616. https://doi.org/10.1002/2017GL074509
Power SB, Casey T, Folland C, Colman A, Mehta V (1999) Inter-decadal modulation of the impact of ENSO on Australia. Clim Dyn 15(5):319–324. https://doi.org/10.1007/s003820050284
Power SB, Delage FPD, Chung CTY, Ye H, Murphy BF (2017) Humans have already increased the risk of major disruptions to Pacific rainfall. Nat Commun 8(1):14368. https://doi.org/10.1038/ncomms14368
Rifai SW, Li S, Malhi Y (2019) Coupling of El Niño events and long-term warming leads to pervasive climate extremes in the terrestrial tropics. Environ Res Lett 14(10):105002. https://doi.org/10.1088/1748-9326/ab402f
Romero D, Alfaro E, Orellana R, Cerda MEH (2020) Standardized drought indices for pre-summer drought assessment in tropical areas. Atmosphere 11(11):1209. https://doi.org/10.3390/atmos11111209
Russell HC (1877) Climate of New South Wales: descriptive, historical, and tabular. Charles Potter, Acting Government Printer
Santoso A, Mcphaden MJ, Cai W (2017) The defining characteristics of ENSO extremes and the strong 2015/2016 El Niño. Rev Geophys 55(4):1079–1129. https://doi.org/10.1002/2017RG000560
Seftigen K, Cook ER, Linderholm HW, Fuentes M, Björklund J (2015) The potential of deriving tree-ring-based field reconstructions of droughts and pluvials over Fennoscandia. J Clim 28(9):3453–3471. https://doi.org/10.1175/JCLI-D-13-00734.1
Singh D, Seager R, Cook BI, Cane M, Ting M, Cook E, Davis M (2018) Climate and the Global Famine of 1876–78. J Clim 31(23):9445–9467. https://doi.org/10.1175/JCLI-D-18-0159.1
Stahle DW, Cook ER, Burnette DJ, Villanueva J, Cerano J, Burns JN, Griffin D, Cook BI, Acuña R, Torbenson MCA, Sjezner P, Howard IM (2016) The Mexican Drought Atlas: tree-ring reconstructions

of the soil moisture balance during the late pre-Hispanic, colonial, and modern eras. Quatern Sci Rev 149:34–60. https://doi.org/10.1016/j.quascirev.2016.06.018

Taschetto AS, Haarsma RJ, Sen Gupta A, Ummenhofer CC, England MH (2010) Teleconnections associated with the intensification of the Australian monsoon during El Niño Modoki events. IOP Conf Ser: Earth Environ Sci 11:012031. https://doi.org/10.1088/1755-1315/11/1/012031

Tejedor E, Saz MA, Esper J, Cuadrat JM, de Luis M (2017) Summer drought reconstruction in northeastern Spain inferred from a tree ring latewood network since 1734. Geophys Res Lett 44(16):8492–8500. https://doi.org/10.1002/2017GL074748

Therrell MD (2005) Tree rings and "El Año del Hambre" in Mexico. Dendrochronologia 22(3):203–207. https://doi.org/10.1016/j.dendro.2005.04.006

Thornthwaite CW (1948) An approach toward a rational classification of climate. Geogr Rev 38(1):55. https://doi.org/10.2307/210739

Tierney JE, Abram NJ, Anchukaitis KJ, Evans MN, Giry C, Kilbourne KH, Saenger CP, Wu HC, Zinke J (2015) Tropical sea surface temperatures for the past four centuries reconstructed from coral archives. Paleoceanography 30(3):226–252. https://doi.org/10.1002/2014PA002717

Torrence C, Compo GP (1998) A practical guide to wavelet analysis. Bull Am Meteor Soc 79(1):61–78. https://doi.org/10.1023/A:1018662703668

van der Wiel K, Matthews AJ, Joshi MM, Stevens DP (2016) Why the South Pacific convergence zone is diagonal. Clim Dyn 46(5–6):1683–1698. https://doi.org/10.1007/s00382-015-2668-0

Vicente-Serrano SM, Beguería S, López-Moreno JI (2010) A multiscalar drought index sensitive to global warming: the standardized precipitation evapotranspiration index. J Clim 23(7):1696–1718. https://doi.org/10.1175/2009JCLI2909.1

Vinod HD, López-de-Lacalle J (2009) Maximum entropy bootstrap for time series: the meboot R package. J Stat Softw 29(5):1–19

Wiedermann M, Siegmund JF, Donges JF, & Donner RV (2021) Differential imprints of distinct ENSO flavors in global patterns of very low and high seasonal precipitation. Frontiers in Climate, 3. https://doi.org/10.3389/fclim.2021.618548

Wilson R, Anchukaitis K, Andreu-Hayles L, Cook E, D'Arrigo R, Davi N, Haberbauer L, Krusic P, Luckman B, Morimoto D, Oelkers R, Wiles G, Wood C (2019) Improved dendroclimatic calibration using blue intensity in the southern Yukon. Holocene 29(11):1817–1830. https://doi.org/10.1177/0959683619862037

Yeh SW, Kug JS, An SI (2014) Recent progress on two types of El Niño: observations, dynamics, and future changes. Asia-Pac J Atmos Sci 50(1):69–81. https://doi.org/10.1007/s13143-014-0028-3

Zhu F, Emile-geay J, Anchukaitis KJ, Hakim GJ, Wittenberg AT, Morales MS, Toohey M, King J (2022) A re-appraisal of the ENSO response to volcanism with paleoclimate data assimilation. Nat Commun 747(13):1–9. https://doi.org/10.1038/s41467-022-28210-1